Chapter 12
Flow Phantoms

Peter R. Hoskins

Learning outcomes

1. Discuss the rationale for the design and use of flow phantoms.
2. Describe optical techniques for visualisation and measurement of flow-fields in flow phantoms (flow visualisation, PI, PTV, LDA).
3. Describe methods of construction of phantoms based on 3D printing, corrosion casting and mould manufacture from milling.
4. Describe the design requirement for phantoms designed for different types of medical imaging.
5. Describe common materials used for the construction of phantoms.
6. Describe methods for formulation of tissue mimic, blood mimic and vessel mimic for flow phantoms used in MRI and ultrasound.
7. Describe the design and use of endothelial flow phantoms.
8. Describe the design and use of whole-artery flow phantoms.

12.1 Introduction to Flow Phantoms

A brief discussion will be presented on the rationale for design and use of flow phantoms. This underpins the remainder of the chapter, however the reader may wish to return to this section once specific examples of flow phantoms have been described.

Flow phantoms are used in the laboratory to mimic the flow of blood in some part of the cardiovascular system in such a manner which allows experiments to be undertaken which would be difficult, or impossible, in the living human. The flow phantom typically consists of a central construct which mimics the geometry of part

P.R. Hoskins (✉)
Edinburgh University, Edinburgh, UK
e-mail: P.Hoskins@ed.ac.uk

P.R. Hoskins et al. (eds.), *Cardiovascular Biomechanics*,
DOI 10.1007/978-3-319-46407-7_12

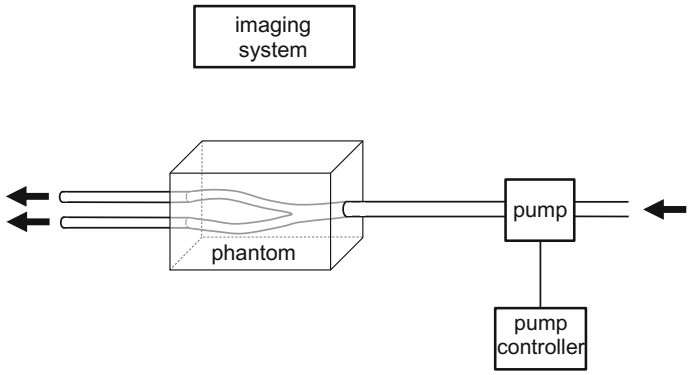

Fig. 12.1 Components of a flow phantom. The phantom mimics the cardiovascular geometry and is connected to a pump by tubing. A pump controller, usually a computer, enables programming of specific flow waveforms. An imaging system is used to record information on blood mimic velocities within the phantom

of the cardiovascular system through which a blood mimic is pumped (Fig. 12.1). An imaging device is used to record information on fluid velocity and related quantities within the central construct.

There are various terms used in the literature including 'experimental flow system', 'phantom' and 'flow phantom'. In this chapter, the term 'phantom' will be used to describe the central cardiovascular construct, and 'flow phantom' used to describe the entire apparatus consisting of pump, pump controller, tubing, reservoirs and the phantom. The phantom consists of components which mainly mimic 2 tissues; the blood (blood mimic) and the soft tissue (tissue mimic). For phantoms mimicking flow in vessels the soft tissue may be further divided into the artery or vein (vessel mimic) and the surrounding soft tissue consisting of fat, muscle, liver, kidney, etc. (tissue mimic).

The advantages of using a flow phantom over an in vivo experiment are:

- *Control.* High degree of control over experimental conditions including vessel geometry and flow rates.
- *Reproducibility.* Ability to undertake repeated experiments with identical experimental conditions.
- *Licensing and safety.* Avoidance of the use of biological material (e.g. blood, arteries, animal models) which may be difficult to obtain, require specialist biological facilities and use-licenses and which may be hazardous.
- *Optical transparency.* Ability to create phantoms which can be used with imaging systems with high temporal and spatial resolution (i.e. optical imaging systems).

The main disadvantage of using a flow phantom over an in vivo experiment is

- *Inadequate mimicking*. The phantom may not adequately mimic the characteristics of the cardiovascular system (e.g. vascular geometry, arterial wall properties, haemodynamics) hence conclusions from experiments may not be applicable in vivo.

The flow phantom replicates or mimics key aspects of the cardiovascular system. The flow phantom cannot mimic in detail all aspects of the cardiovascular system. One might then ask: how complicated does the flow phantom need to be? As with computational models discussed earlier (Chap. 10), the flow phantom needs to be sufficiently complex to allow a specific research question to be answered. This rationale then dictates that the research question comes first, and the flow phantom design follows the research question. If the research question changes then this may require redesign of aspects of the flow phantom. Another way of expressing this rationale is that the flow phantom is a simplified version of reality. The design of the flow phantom needs to be as complicated as necessary and no more complicated than that. An overcomplicated flow phantom will mean unnecessary effort in construction. It is noted that a similar rationale was discussed in Chap. 10 on the complexity of the computational model.

There are three main uses of flow phantoms:

- *Investigation of flow-field velocity data and associated phenomena*. Optical imaging systems such as PIV (particle image velocimetry) and LDA (laser Doppler anemometry) have high spatial and temporal resolution and have been mostly used for measurement of flow-field velocity data and associated phenomena.
- *Validation of flow-field data obtained using medical imaging*. Medical imaging systems such as MRI and ultrasound can be used to measure blood velocity and associated quantities. Validation of measured velocity is commonly undertaken using flow phantoms.
- *Investigation of the relationship between flow and aspects of biological function of the vessel wall*. These flow phantoms are mostly concerned with endothelium which is cultured on the walls of a flow chamber where the relationship between wall shear rate and endothelial function is of interest.

12.2 Optically Transparent Phantoms

The use of an optically transparent phantom allows direct visualisation of flow patterns and measurement using optical techniques. This section will describe phantom construction and the associated optical imaging techniques. Further reading of optical techniques with respect to use in medical applications is given in the reviews by Hoskins (2008) and Vennemann et al. (2007).

12.2.1 Flow Visualisation

This is the simplest method for investigating flow patterns. The flow is seeded with a material which ideally is neutrally buoyant and can be visualised. Materials which have been used include injected dyes and inks, hydrogen bubbles, hollow glass spheres and a variety of solid particles. The seeded material will follow the flow-streamlines allowing the observer to visualise flow patterns. A video camera can be used to record the progress of the seeded material. In Fig. 1.18 a simple straight tube phantom with dye injection illustrated the difference between laminar flow and turbulence. Phantoms with anatomical geometry provided early evidence of complex flow patterns in bifurcations, including flow recirculation and helical flow (Ku and Giddens 1983; Zarins et al. 1983) (Fig. 12.2). Flow visualisation as its name implies is only concerned with qualitative visualisation of flow patterns, not quantitative measurement of velocities.

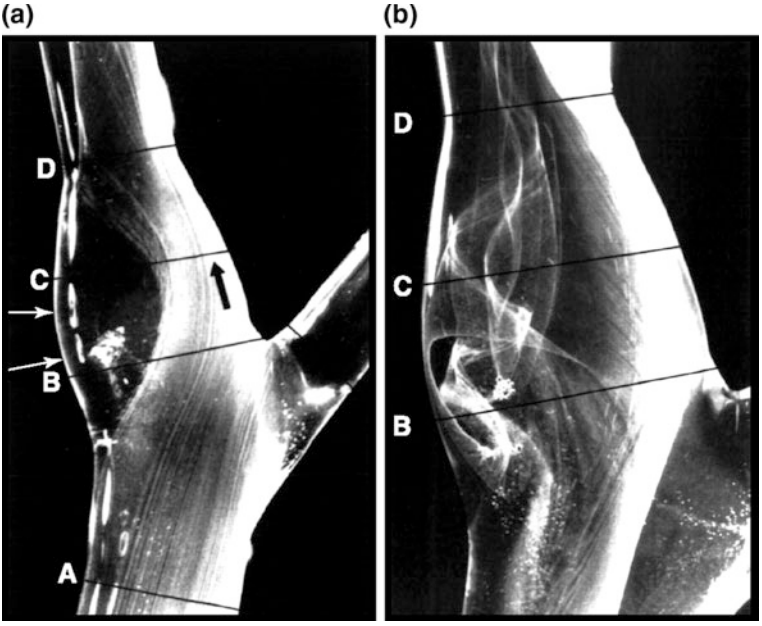

Fig. 12.2 Flow visualisation in a model of the carotid bifurcation. From;Zarins CK, Giddens DP, Bharadvaj BK, Sottiurai VS, Mabon RF, Glagov S; Carotid bifurcation atherosclerosis. Quantitative correlation of plaque localization with flow velocity profiles and wall shear stress; Circulation Research 1983;53(4):502–514; reprinted with permission by Wolters Kluwer Health, Inc. Circulation Research is an official journal of the American Heart Association

12.2.2 Particle Image Velocimetry (PIV) and Particle Tracking Velocimetry (PTV)

Quantitative measurement of the velocity field may be undertaken using particle image velocimetry (PIV). In PIV the fluid is seeded with particles at low concentration of typically less than 1 % by volume. A pulsed laser is used to illuminate a single plane within the flow. A video camera is used to record sequential images of the illuminated particles. Between images the particles move a small distance. Image processing algorithms applied to groups of particles are used to estimate the distance the particles have moved; this distance is divided by the time between images to obtain the local velocity. Figure 12.3 shows an example of PIV data taken in a stenosis phantom. A related technique is particle tracking velocimetry (PTV) in which individual particles are tracked rather than groups of particles. Further details of PIV and PTV technology are provided by Adrian (1991), Westerweel (1997) and Prasad (2000).

PIV provides high accuracy high resolution data on the velocity field. Due to its simplicity, accuracy and robustness it is regarded as providing gold-standard data, which is useful in validation of flow-field data obtained from CFD or from medical imaging.

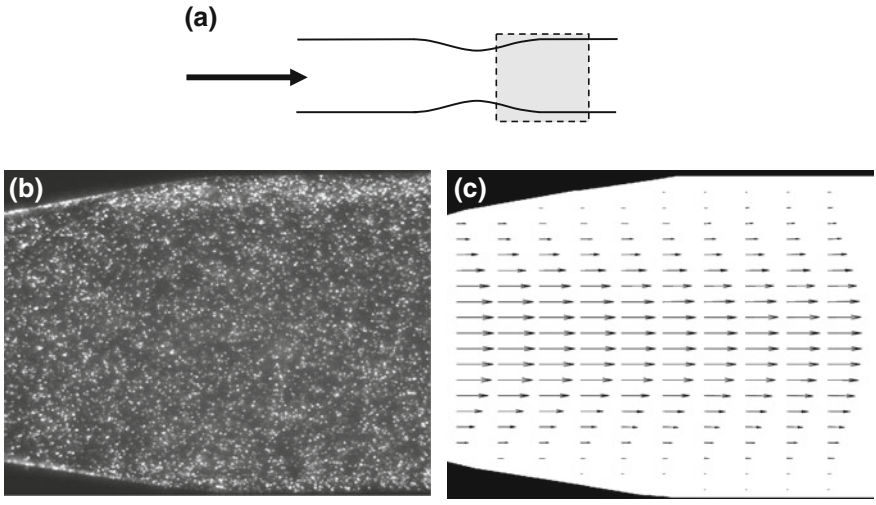

Fig. 12.3 PIV in a stenosis model. **a** The interrogation region is shown as shaded in the schematic. **b** A typical PIV image; each bright dot represents a particle or group of particles. **c** Estimated velocity field

12.2.3 Laser Doppler Anemometry (LDA)

Quantitative measurement of velocity may also be undertaken using laser Doppler anemometry (LDA). Two laser beams of the same frequency overlap producing a set of interference fringes within the overlap region. Particles moving through the interference fringes scatter light. The scattered light is detected by a photodetector. The frequency of the scattered light is dependent on the velocity of the particle and also on the angle between the direction of motion and the laser interference wave direction. This is very similar to Doppler ultrasound in that the motion of a particle produces a Doppler frequency shift. Common positions for the detector are on the opposite side to the laser or on the same side. Use of a single detector enables measurement of one velocity component whereas use of multiple detectors allows measurement of two or three velocity components. Information is gathered at a single point, however 3D information may be obtained by scanning the interrogation region through the flow field. Information is gathered continuously so that LDA may be used to study high frequency changes in the flow field associated with turbulence. Further details of LDA technology are provided by Tropea (1995); Liepsch et al. (1998) reviews the use of LDA in carotid artery phantoms.

12.2.4 Phantom Construction

Materials which are optically transparent and which have been used for phantom manufacture include glass, acrylic, polyester and silicone elastomers. The use of glass is challenging requiring phantom manufacture using glass-blowing. Most optically transparent phantoms with complex vascular geometries are manufactured using polyester, acrylic or silicone elastomers using a casting technique involving pouring and setting of the liquid. A simple straight tube model may be manufactured using metal rods which are joined together. These rods are positioned in a box and the liquid is poured into the box, allowed to set and the rods removed (Fig. 12.4).

3D cardiovascular geometries such as bifurcations require a more complicated manufacturing approach. Phantom manufacture is increasingly dominated by recent

Fig. 12.4 Straight-tube stenosis phantom for use in PIV. The metal rods used in construction are shown positioned within the phantom

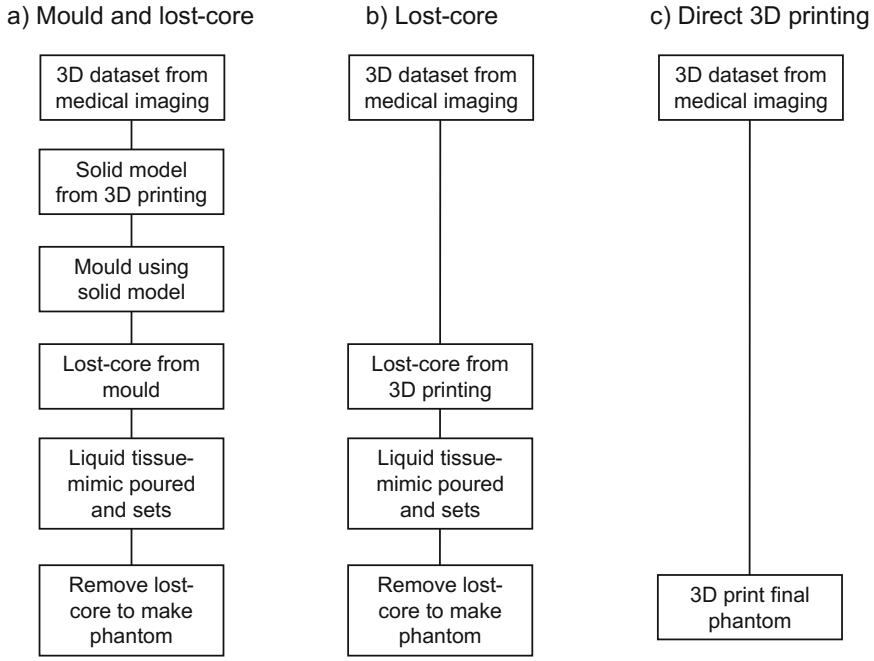

Fig. 12.5 Steps in the manufacture of 3D phantoms using 3D printing. **a** Mould and lost core. **b** Lost core. **c** Direct 3D printing

developments in rapid-prototyping (3D printing). Figure 12.5 summarises the steps which have been taken in published studies and are described below.

- *Mould and lost core.* This method is exemplified by Watts et al. (2007). A 3D dataset of the carotid bifurcation is obtained from a volunteer using MRI. This is used to generate an idealised CAD (computer-aided design file) in which surfaces are smoothed and some arterial segments straightened (Fig. 12.6a). A solid model of the bifurcation is 3D printed. This is used to make a mould consisting of silicone. A low melting point alloy is poured into the mould. After cooling, the metal core is removed (Fig. 12.6b) and incorporated into a container with suitable inlet and outlet connections. Liquid silicone elastomer is poured into the box and allowed to set. Once set the container is heated resulting in melting of the metal core which can then be poured out leaving the final phantom containing the anatomical geometry (Fig. 12.6c). Doyle et al. (2008) also describes this process step by step for use in creating abdominal aortic aneurysm phantoms.
- *Lost core.* This method is exemplified by Geoghegan et al. (2012). The procedure is similar to that described above except the steps involving the mould are missing. The lost core is 3D printed directly. The lost core is composed of water-dissoluble plaster powder. This is coated with PVA which provides

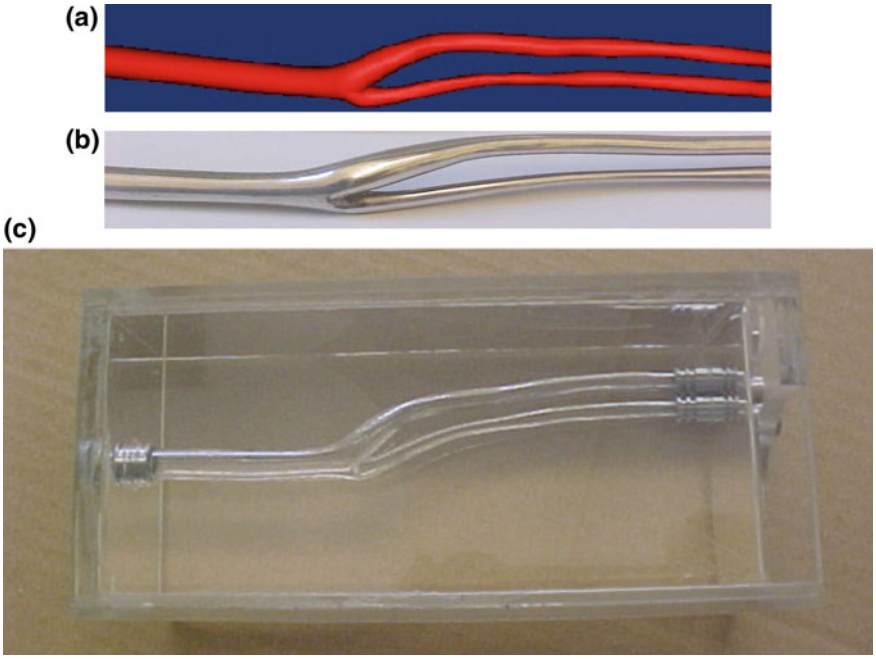

Fig. 12.6 Bifurcation phantom for use in optical studies manufactured using the 'mould and lost core' approach. **a** CAD image. **b** Lost core. **c** Final phantom. See Watts et al. (2007) for more detail

smoothness, strength and acts to prevent ingress of the liquid silicone elastomer. After the elastomer has set the core is removed through a combination of water and physical erosion with a soft scraper, producing the final phantom (Fig. 12.7).

- *Direct 3D printing*. This represents one of the goals in phantom manufacture as the number of steps is reduced to the minimum; direct 3D printing of the phantom in final form. Cloonan et al. (2014) describes the use of 3D printing for phantom manufacture.

Other methods have been used to acquire 3D geometries and create phantoms:

- *Corrosion casting* of arteries involves injection of a liquid into autopsy or excised tissues. The liquid hardens in the artery and the tissues are chemically removed. Early studies on anatomical optical phantoms used injected silicone rubber which then formed the lost core in a phantom consisting of transparent plastic (Friedman et al. 1987; Friedman 1993). Resin-based corrosion casting is commonly used producing a high-resolution stiff model of the vascular system. Whilst this could not be removed using a lost core method, the model geometry could be scanned using a laser scanning system to provide a 3D CAD file

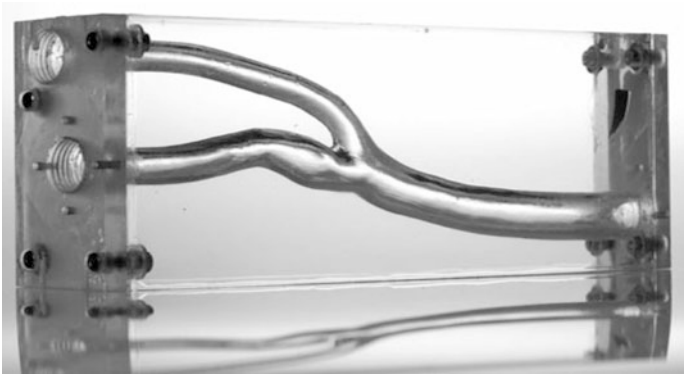

Fig. 12.7 Carotid artery bifurcation rigid flow phantom. The phantom is for use in optical studies manufactured using the 'lost core' approach. From; Experiments in Fluids; Fabrication of rigid and flexible refractive-index-matched flow phantoms for flow visualisation and optical flow measurements; Vol. 52, 2012, pp. 1331–1347, Geoghegan P, Buchmann N, Spence C, Moore S, Jermy M; © Springer-Verlag 2012, with permission of Springer

suitable for 3D printing. 3D geometry data obtained from corrosion casting of arteries is extremely high quality.

- *Mould manufacture from milling*. Planar anatomical phantoms have been manufactured based on the lost core method (Smith et al. 1999) which have been used in flow visualisation (Steinman et al. 2000). An idealised planar carotid bifurcation was used from which a mould was made in aluminium using a milling machine. The mould was used to produce a lost core in low melting point alloy from which the phantom was produced in silicone.

Once the phantom has been produced, the blood mimic must be designed to match the refractive index of the material of the phantom (Nguyen et al. 2004; Miller et al. 2006; Yousif et al. 2011) otherwise there will be visualisation artefacts (Fig. 12.8) and velocity measurement errors.

12.3 Flow Phantoms for Medical Imaging

12.3.1 Medical Imaging Flow Phantom Design Requirements

Flow phantoms for medical imaging should mimic key features of the cardiovascular system which, as discussed above will depend on the application. Features might include cardiovascular geometry, blood viscous behaviour, wall stiffness and wall motion. In addition flow phantoms should mimic key properties of tissue relevant to the imaging modality. This ensures that images produced from the

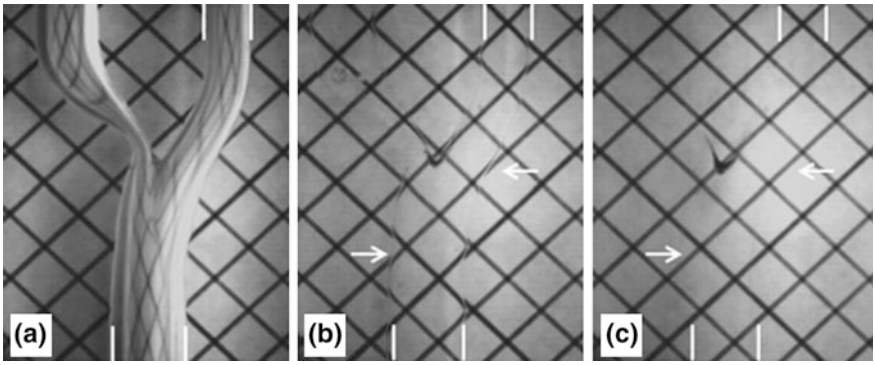

Fig. 12.8 Visual monitoring of the match in optical refractive index based on distortion of grid lines beneath a carotid bifurcation phantom fabricated from polydimethylsiloxane (PDMS) polymer. The phantom is filled with **a** air, showing high distortion, **b** nearly matched fluid ($n = 1.4112 \pm 0.0001$), still showing minor distortion as indicated by the *arrows*, and **c** optimally matched fluid ($n = 1.4140 \pm 0.0001$) with no distortion, as indicated by the *arrows*. Note the *vertical white markers*, denoting the flow lumen, and the unintentional stain at the bifurcation apex, which provides a convenient landmark here. From Yousif et al. (2011); © Springer-Verlag 2010, with permission of Springer. Image kindly provided by Prof. Tamie Poepping

Table 12.1 Relevant physical properties of materials relevant to flow phantom design

Imaging system	Physical properties relevant to imaging
MRI	T1, T2, proton density
Ultrasound	Speed of sound, acoustic attenuation, acoustic backscatter coefficient
CT	X-ray attenuation coefficient
PET	Gamma-ray attenuation coefficient

phantom are a good representation of images from the cardiovascular system in vivo. Tissue-mimicking also enables conclusions (e.g. on quantification of measurement errors) to be applicable in vivo. Construction of flow phantoms for medical imaging therefore requires choice or formulation of materials with the correct physical properties.

Materials which mimic the relevant imaging properties of tissues are referred to as being 'tissue equivalent'. The relevant imaging properties are summarised in Table 12.1.

12.3.2 Tissue and Vessel Mimics

The most commonly used phantoms consist of a length of tubing bought from a laboratory supplier. Stiff tubing includes acrylic, glass, PTFE and polypropylene, whilst softer tubing is mostly based on latex rubber. These simple vessel phantoms

may be used to produce idealised flow to validate MRI velocity measurement methods; with the implication that the MR properties of the tube are unimportant as they have little effect on the measurement of velocity. Simple tube models have been used in ultrasound, however the tube has a large effect due to refraction and attenuation of the ultrasound beam within the vessel wall. C-flex tubing (Cole Parmer, Vernon Hills, IL, USA) has been used as its speed of sound (1556 m s^{-1}) is close to the standard speed of 1540 m s^{-1} (Hoskins 2008).

Off-the-shelf materials can also be used to construct medical imaging phantoms with more complicated geometries. For CT and PET solid materials such as acrylic provide similar X-ray and gamma-ray attenuation characteristics to human tissue. This is convenient as phantoms can easily be constructed by milling or by casting. For MRI solid materials such as polyester, acrylic or silicone have been used to construct phantoms (e.g. Smith et al. 1999). Essentially these phantoms are identical to those used for optical imaging (Sect. 12.1). Figure 12.9 shows bifurcation phantoms and the associated MRI images of flow.

Solid materials such as polyester do not return an MRI signal which leads to unrealistic image appearance (Smith et al. 1999). This is an issue if the effect of surrounding tissue on velocity measurement is of interest. Solid materials such as acrylic have high speed of sound compared to soft tissue and are unsuitable for use in ultrasound phantoms. Ultrasound phantoms are available commercially based on urethane as the acoustic properties provide a reasonable match for soft tissue (Table 12.2).

Use of off-the-shelf materials is unlikely to lead to tissue mimics with the correct MRI or acoustic properties simply because these materials are not primarily designed for use as tissue mimics. Better success has been achieved by formulating recipes based on chemicals. Recipes based on agar have been used for both MRI and ultrasound tissue mimics which have good matching of acoustic and MRI properties (Tables 12.2 and 12.3). For use in MRI the agar is doped with a paramagnetic ion such as gadolinium, manganese, copper or nickel. The agar mixture is cooked for several hours, allowed to cool and poured. As it sets cross-linking of polymer molecules occurs which stabilises the agar. The cross-linking also leads to thermal irreversibility in that the melting temperature is higher (by 10–20 °C) than the setting temperature. This feature is essential when agar is used in lost core phantom construction; the liquid agar tissue mimic must not melt the alloy core; yet when the temperature is raised the alloy core must melt while the agar tissue mimic remains solid. The widely used agar tissue mimic developed by Tierlinck et al. (1998) has very good acoustic matching to soft tissue but is mechanically weak which can lead to phantom rupture (Meagher et al. 2007). A recipe based on konjac and carogeenan leads to higher mechanical strength enabling phantoms to be built without rupture (Meagher et al. 2007; Kenwright et al. 2015).

A second approach for the formulation of tissue mimics for MRI and ultrasound is the use of polyvinyl alcohol (PVA). This is initially prepared as a gel (Mano et al.

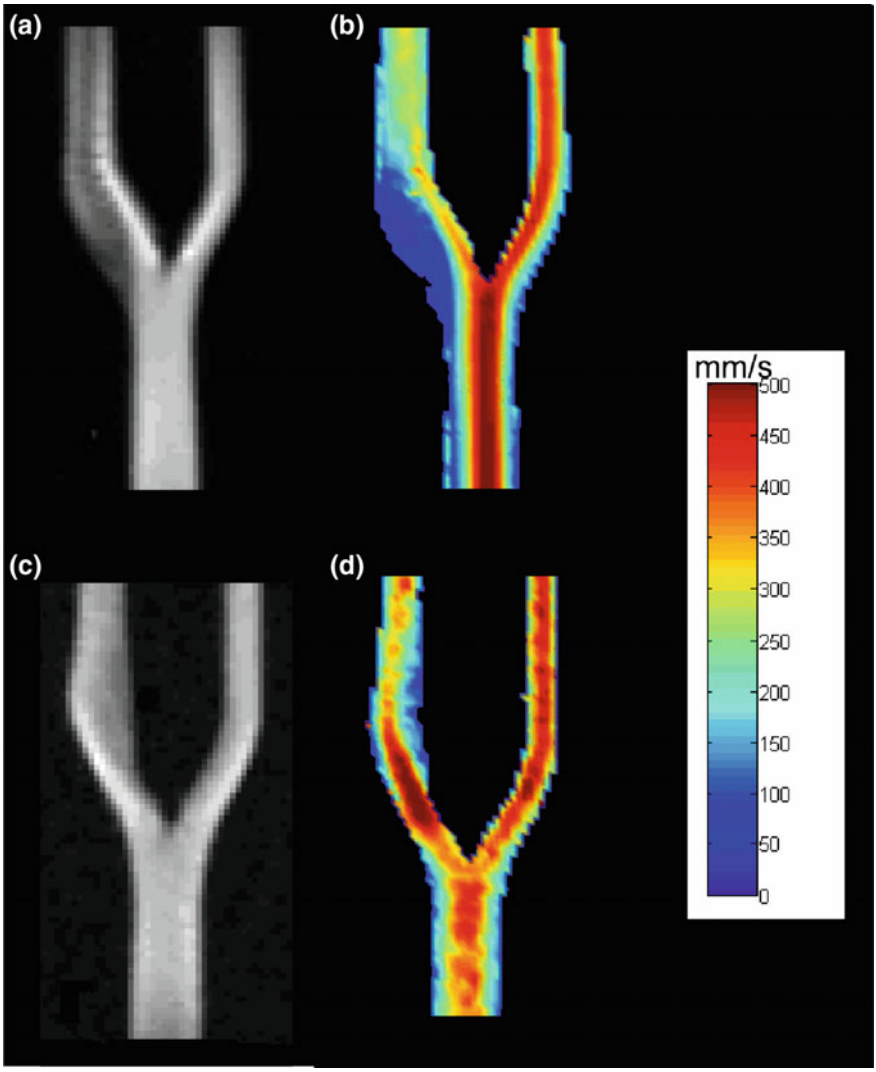

Fig. 12.9 MRI images from bifurcation phantoms. **a** Normal phantom—MRI intensity. **b** Normal phantom—MRI velocity. **c** 30 % stenosis phantom—MRI intensity. **d** 30 % stenosis phantom—MRI velocity. From; Marshall I. Computational simulations and experimental studies of 3D phase-contrast imaging of fluid flow in carotid bifurcation geometries. Journal of Magnetic Resonance Imaging. 2010;31:928–934; © 2010 Wiley-Liss, Inc., with permission from John Wiley and Sons. Images kindly provided by Prof. Ian Marshall

1986; Chu and Rutt 1997) which then undergoes a series of freeze-thaw cycles producing a white elastic material known as PVA cryogel or PVAc. The process of freeze-thawing results in cross-linking of the PVA polymer molecules. The number

Table 12.2 MRI properties of selected tissue mimics, vessel mimics and blood mimics

Mimic/Tissue	Main composition	T1 (ms) @1.5T	T2 (ms) @1.5T	T1 (ms) @3T	T2 (ms) @3T	Reference
Tissue/Vessel	PVAc (10 %)	718–1034[a]	108–175[a]	–	–	Surry et al. (2004)
Tissue	Agar	1150	50	1504	40	Smith et al. (1999), King et al. (2011)
Tissue	Sodium polyacrylate	–	–	1077–2406	74–602	Hellerbach et al. (2013)
Tissue	Carrageenan/Agarose	202–1904	38–423	395–2601	29–334	Kato et al. (2005), Hattori et al. (2013)
Soft tissues	–	576–1124	44–95	812–1820	42–99	Selwyn (2014)
Blood	–	1441	290	1932	275	Selwyn (2014)
Blood	60:40 by vol water/glycerol	900	125	–	–	Summers et al. (2005)

[a]Values depend on number of freeze-thaw cycles

Table 12.3 Acoustic properties of selected tissue mimics, vessel mimics and blood mimics. Values reported for clinical frequency range (5–15 MHz). FT—free-thaw cycle

Mimic	Main composition	Velocity (m s^{-1})	Attenuation coefficient (dB cm^{-1} MHz^{-1})	Reference
Tissue	Agar	1551	0.52	Tierlinck et al. (1998)
Tissue	Konjac-carrageenan	1549	0.47	Kenwright et al. (2015)
Tissue/Vessel	PVAc	1543–1583[a]	0.18–0.42[a] (at 5 MHz)	Dineley et al. (2006)
Tissue	Urethane	1465	0.9 (at 5 MHz)	Browne et al. (2003)
Vessel	C-flex (Cole-Parmer)	1556	5.6 (at 5 MHz)	Hoskins (2008)
Vessel	Photopolymer	1802	1.58	Lai et al. (2013)
Ideal tissue[b]	–	1540	0.5	IEC 61685
Ideal blood[b]	–	1570	<0.1	IEC 61685
Blood mimic	Glycerol-water-nylon	1548	0.05	Ramnarine et al. (1998)

[a]Value depend on number of freeze-thaw cycles
[b]IEC specification for standard tissue and blood mimic (IEC 2001); allowed tolerances are 1 % for speed of sound and 10 % for attenuation coefficient

of freeze-thaw cycles is used to control acoustic and MRI properties (Tables 12.2 and 12.3). The PVAc tissue mimic has high mechanical strength and is capable of withstanding physiologic pressure. PVAc is suitable for manufacture of a vessel wall mimic (Surry et al. 2004; Dineley et al. 2006).

12.3.3 Blood Mimics

It is common practice to design blood mimics with a viscosity of 3–4 mPa s with the intention that these behave in a Newtonian manner. For MRI a mixture of liquids with a high water content such as a 40/60 solution by mass of glycerol/water provide good blood mimicking (Smith et al. 1999; Summers et al. 2005). For ultrasound use of pure fluid does not work as particles are required to generate acoustic scatter. The blood mimic developed by Ramnarine et al. (1998) has been widely used. This is a glycerol/water fluid mixture with 5 μm nylon particles added in low concentration (1.8 % by volume) to mimic red blood cells and dextran to ensure matching of viscosity to blood.

Table 12.4 Methods for manufacture of MRI and ultrasound phantoms at increasing levels of complexity

	MRI	Ultrasound
Straight tube: (not tissue equivalent)	[a]Off-the-shelf vessel[1]	[a]C-flex tubing[2]
Straight tube: (tissue equivalent)	[b]PVAc vessel mimic[3]	[b]PVAc vessel mimic[4]
		[b]Agar block with channel[5]
Planar bifurcation: (not tissue equivalent)	[b]Machined acrylic[6]	Not applicable
	[b]Lost core made in planar mould, silicone elastomer tissue mimic[7]	
Planar bifurcation: (tissue equivalent)	[c]Lost core made in planar mould, agar based tissue mimic[7]	[c]Lost core made in planar mould, agar based tissue mimic[7]
Nonplanar bifurcation phantom: (not tissue equivalent)	[c]Direct 3D printing of vessel mimic in photopolymer tissue, embedded in agar tissue mimic[8]	Not applicable
Nonplanar bifurcation geometry: (tissue equivalent)	[c]Lost core made by 3D printing, agar based tissue mimic	[c]Lost core made by 3D printing, konjac-carogeenan tissue mimic[9]
	[d]Direct 3D printing	[d]Direct 3D printing

Difficulty [a]very easy (commercially available), [b]easy (commercially available or specialist in-house facilities), [c]difficult (specialist in-house facilities), [d]very difficult (very few/no reports)
References [1]Robertson et al. (2001), [2]Blake et al. (2008), [3]Surry et al. (2004), [4]Dineley et al. (2006), [5]Ramnarine et al. (2001), [6]Kohler et al. (2001), [7]Smith et al. (1999), [8]Lai et al. (2013), [9]Watts et al. (2007), Meagher et al. (2007)

12.3.4 Phantom Construction

In principle all of the methods described in Sect. 12.2.4 can be used for the construction of medical imaging phantoms. A summary of methods used for phantoms of increasing geometric complexity is shown in Table 12.4, concentrating on MRI and ultrasound.

The simplest phantom, and the most widely used, consists of off-the-shelf tubing bought from laboratory suppliers. For ultrasound, as noted above, C-flex tubing provides adequate acoustic matching. Off-the-shelf tubing can be arranged to be straight, and provided the inlet is sufficiently long, the flow is fully developed. This allows comparison of measured velocities with the true velocity within the vessel (Robertson et al. 2001; Blake et al. 2008). The next level of complexity also involves straight tube phantoms but with tissue equivalence of the vessel. PVAc may be used for both MRI and ultrasound phantoms (Surry et al. 2004; Dineley et al. 2006), or a wall-less approach may be used involving agar tissue mimic for ultrasound (Ramnarine et al. 2001). Figure 12.10 shows ultrasound images taken from a wall-less stenosis phantom.

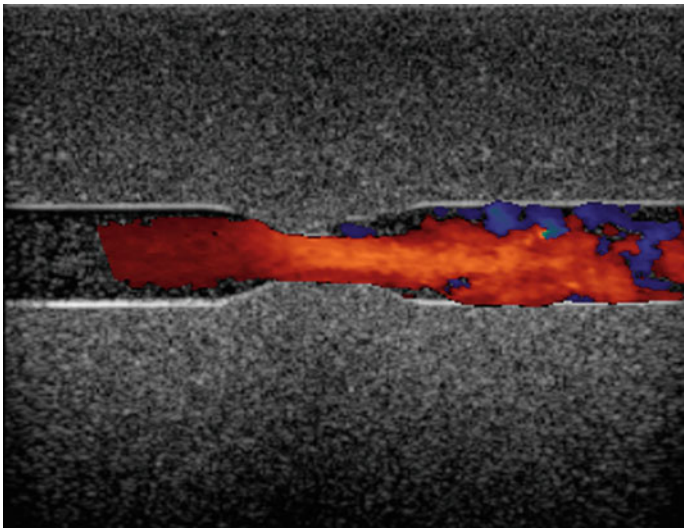

Fig. 12.10 Straight tube wall-less stenosis phantom. *Colour* Doppler image showing increase in velocity in the stenosis with turbulent flow in the post-stenosis region

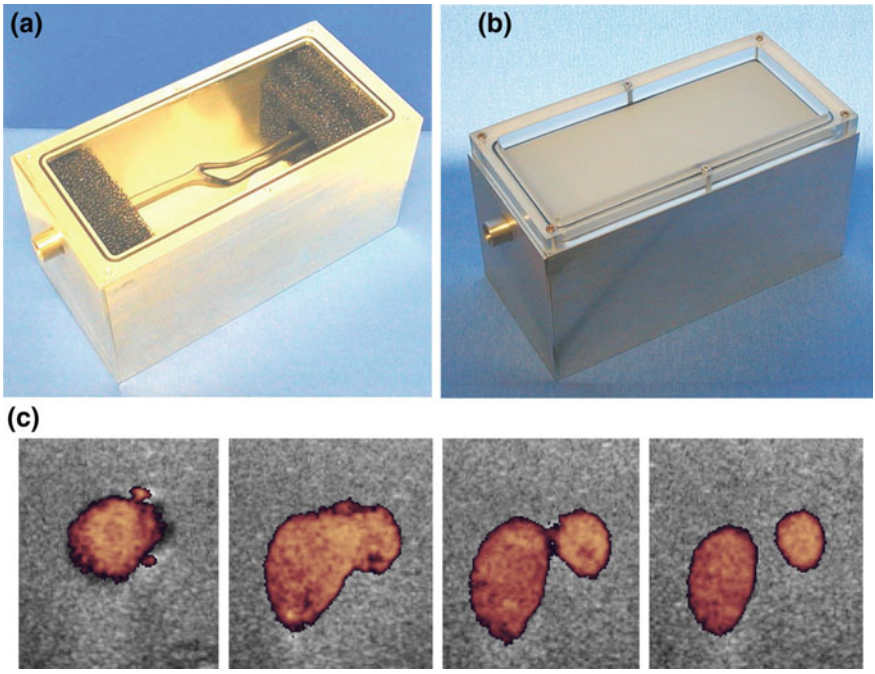

Fig. 12.11 Ultrasound carotid bifurcation phantom. **a** The lost core in a container with inlet and outlet connections in place. **b** Final phantom with solid tissue mimic after the metal core has been removed. **c** Cross-sectional colour flow images at 4 locations. Further details in Meagher et al. (2007) and Watts et al. (2007)

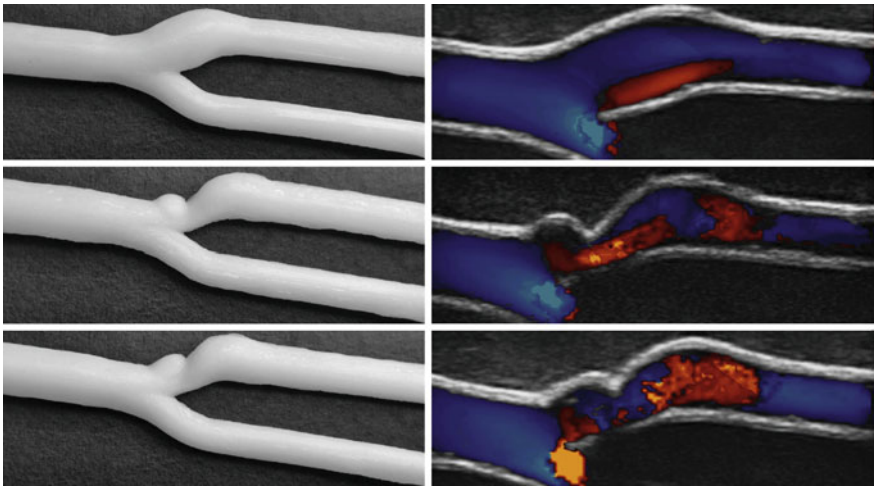

Fig. 12.12 **a** 3D-printed carotid bifurcations vessel mimics. **b** *Colour* flow images from the phantoms. Reprinted from Lai et al. (2013), copyright (2013), with permission from the World Federation for Ultrasound in Medicine & Biology

Planar bifurcations may be manufactured for MRI using machined acrylic; i.e. circular holes are bored which meet at the bifurcation (Kohler et al. 2001), or using a lost core mould as described in Sect. 12.2.4 (Smith et al. 1999). Tissue equivalent versions of these phantoms can be made by using agar (a jelly-like substance derived from a naturally occurring complex polysaccharide) (Smith et al. 1999).

The final level of complexity concerns 3D anatomical phantoms and involves the use of 3D printing (Watts et al. 2007; Meagher et al. 2007; Lai et al. 2013) as shown in Figs. 12.11 and 12.12. Direct 3D printing of 3D anatomical phantoms for ultrasound and MRI would require materials suitable for 3D printing.

12.4 Biological Flow Phantoms

This class of flow phantoms incorporates biological tissues and allows exploration of the relationship between biological function and local haemodynamic and mechanical conditions. As with the other sections in this chapter, we will concentrate on the design and construction of the phantoms.

12.4.1 Brief History of Endothelial Flow Phantoms

It has been recognised for over 150 years that the endothelium senses haemodynamic forces (Virchow 1856). Flow systems for the systematic study of these effects in the laboratory date back to the 1970s (Krueger et al. 1971; Rosen et al. 1974). Studies in the early 1980s demonstrated alignment of endothelial cells with the direction of wall shear stress (Dewey et al. 1981; Levesque and Nerem 1985). The basis for these studies was a flow chamber in which endothelial cells were cultured on one wall. Flow through the chamber subjected the cells to a controllable shear stress. The transparent walls of the chamber allowed optical visualisation using microscopy which enabled examination of the behaviour of the endothelial cells under different shear conditions. Since these early studies cultured endothelial flow chambers have become by far the most widely used method for investigating endothelial response to shear stress. The terms 'endothelial flow cell' and 'cell culture flow system' are also used to describe the flow apparatus. For the purposes of consistency the term 'endothelium flow phantom' is used in this chapter. Reviews of the design of endothelial flow phantoms are provided by Young and Simmons (2010) and Davis et al. (2015), and of biological use are provided by Davies (1995, 2009).

12.4.2 Endothelial Flow Phantom Design

The components of an endothelial flow phantom are shown in Fig. 12.13 based on the popular parallel plate flow chamber. The flow chamber consists of three layers, a lower plate on which the endothelial cells are seeded, a gasket which defines a flow channel and an upper plate which seals the flow channel.

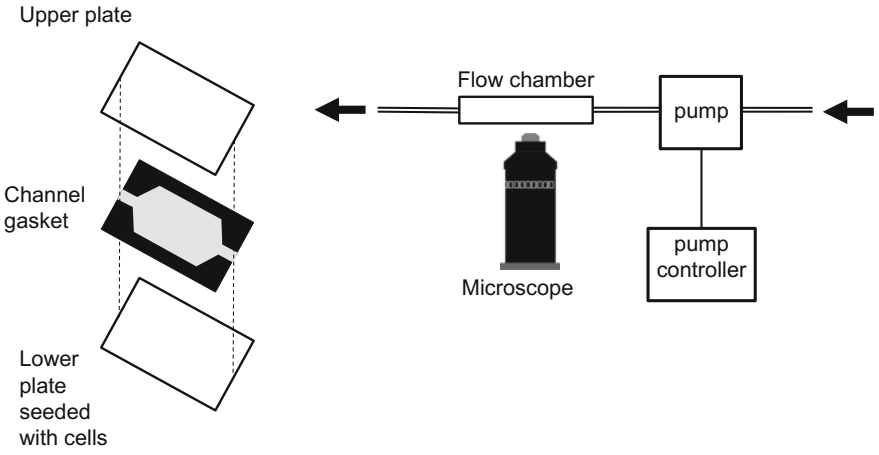

Fig. 12.13 Components of a parallel plate endothelial flow phantom

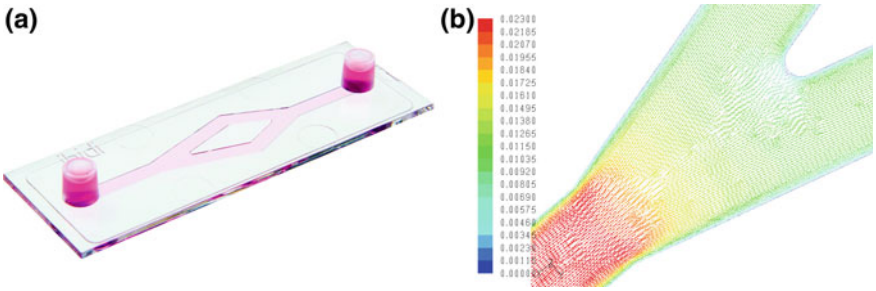

Fig. 12.14 **a** Y-shaped parallel plate endothelial flow phantom. **b** Velocity field estimated using CFD. Images provided courtesy of Ibidi GmbH (Martinsried, Germany)

The components of a simple parallel plate flow phantoms are described in more detail below.

- *Endothelial plate.* The endothelial cells are most commonly seeded onto glass or glass-like materials which are rigid. If coated direct onto the glass the endothelial cells need time to lay down their own matrix to allow adherence to the glass. The use of a plate surface coating such as fibronectin, collagen or gelatin assists with cell adherence. The endothelial cells form a single-cell layer in which there are no gaps (called a 'confluent layer').
- *Opposite plate.* In simple flow chambers the opposite plate is constructed of glass to allow optical access.
- *Flow chamber geometry.* The basic flow chamber is designed so that fully developed flow is present. A step may be introduced into the flow to simulate the complex flow regions seen in atherosclerosis. More complex geometries may be constructed such as the Y-shaped geometry available from Ibidi GmbH (Martinsried, Germany) (Fig. 12.14). It is important to have good knowledge of the shear stress. This may be calculated for different flow rates using simple equations for simple geometries such as rectangular cross sections. For more complex geometries CFD may be used to estimate the shear stress distribution (Fig. 12.14).
- *Pump.* Simple experiments may be performed using steady flow, for example produced using a syringe pump. Physiological flow involving pulsatile flow requires a more sophisticated system with computer control of the pump speed.
- *Fluid.* The fluid used in endothelial flow phantoms is designed to replicate the osmotic and ion concentrations of fluid in the body, in this case of the plasma component of blood. Typically a general purpose fluid used in biological research called 'phosphate buffered saline' is used. This fluid mimics the osmolarity and pH of tissue fluid.
- *Microscope.* Simple visualisation of endothelial cells may be performed using an optical microscope. More detailed information on biological processes may be obtained using a variety of fluorescence techniques.

There have been many variants of the simple endothelial flow phantom described, some of which are detailed below (reviewed in Young and Simmons 2010).

- *Cone-plate phantom.* The cone-plate viscometer described in Chap. 3 provides a uniform shear distribution and also enables variation of shear over a wide range. This methodology can be included in an endothelial flow phantom. The cone may be optically transparent allowing microscope visualisation of the endothelial layer through the cone.
- *Combined flow-stretch-pressure phantom.* In vivo endothelial cells are subject to simultaneous changes in pressure, stretch and shear. Endothelial phantoms have been described in which the endothelial cells are subjected to two or three of these variables. To allow for stretching, endothelial cells are seeded onto nonrigid materials such as silicone.
- *Co-culture phantom.* In vivo endothelial behaviour in an artery is affected by smooth muscle cells. In a co-culture phantom the endothelial cells and smooth muscle cells are both seeded and cultured. For example, separation of endothelial and smooth muscle cells is achieved by culturing them on opposite sides of a membrane.
- *Microfluidics.* Microfluidics refers to the set of techniques concerned with construction of devices which utilise movement of tiny amounts of fluid. These techniques are increasingly used to construct endothelial flow phantoms. There are two main reasons for this; one is the ability to run several experiments in parallel, all with either the same or slightly different conditions (hence vastly speeding up the process of experimentation). The second reason is the large reduction in the volume of consumables which are needed (hence reducing cost). A typical endothelial flow phantom constructed using microfluidic procedures might have a 100-fold reduction in endothelial surface area compared to a conventional phantom; with typical dimensions of 1 by 10 mm.

12.4.3 Whole-Artery Phantoms

These phantoms are composed of sections of excised artery which are plumbed into a flow network which can replicate key aspects of the in vivo haemodynamic and mechanical environment, including pressure, stretch and wall shear. These phantoms have several advantages over in vivo experiments

- *Biological behaviour.* The biological behaviour should be very similar to that in vivo as the artery is composed of the same cells that exist in vivo. It has been noted above that there is biological signalling between endothelial cells and smooth muscle cells which is naturally replicated in a whole-artery phantom. It has been argued that endothelial cells used in endothelial flow phantoms may have a nontypical phenotype hence their behaviour differs to the in vivo situation (Bergh et al. 2005)

- *Independent control of mechanical environment.* In vivo endothelial cells are subject to simultaneous changes in pressure, stretch and shear. In a whole-artery phantom it is possible to have independent control of pressure, stretch and shear. It is noted that this argument is also applicable to endothelial phantoms.

The principal disadvantage is that the artery is not optically transparent hence use of conventional microscopy techniques which image through the container wall is not possible.

The metabolic activity of the artery is maintained by immersion in a fluid which has appropriate levels of ions, glucose, oxygen and carbon dioxide. Dextran may be added to the blood mimic to control viscosity. Whole-artery flow phantoms have been described by Gan et al. (1999), Han and Ku (2001), Bergh et al. (2005), Gambillara et al. (2006), Thacher et al. (2010), Ozaki and Karaki (2002) provides a review of work to 2001.

References

Adrian RJ. Particle-imaging techniques for experimental fluid-mechanics. Ann Rev Fluid Mech. 1991;23:261–304.

Bergh N, Ekman M, Ulfhammer E, Andersson M, Karlsson L, Jern S. A new biomechanical perfusion system for ex vivo study of small biological intact vessels. Ann Biomed Eng. 2005;33:1808–18.

Blake JR, Meagher SC, Fraser KH, Easson WJ, Hoskins PR. A method to estimate wall shear rate with clinical ultrasound scanners. Ultrasound Med Biol. 2008;34:760–74.

Browne JE, Ramnarine KV, Watson AJ, Hoskins PR. Assessment of the acoustic properties of common tissue-mimicking test phantoms. Ultrasound Med Biol. 2003;29:1053–60.

Chu KC, Rutt BK. Polyvinyl alcohol cryogel: An ideal phantom material for MR studies of arterial flow and elasticity. Magn Res Med. 1997;37:314–9.

Cloonan A, Shammirzadi D, Li RX, Doyle BJ, Konoafagou EE, McGloughlin TM. 3D-printed tissue mimicking phantoms for medical imaging and computational validation studies. 3D Printing Add Manuf. 2014;1:14–23.

Davies PF. Flow-mediated endothelial mechanotransduction. Physiol Rev. 1995;75:519–60.

Davies PF. Hemodynamic shear stress and the endothelium in cardiovascular pathophysiology. Nat Clin Pract Cardiovasc Med. 2009;6:16–26.

Davis CA, Zambrano S, Anumolu P, Allen AC, Sonoqui L, Moreno MR. Device-based in vitro techniques for mechanical stimulation of vascular cells: a review. J Biomech Eng. 2015;137:040801. doi:10.1115/1.4029016. Epub 5 Feb 2015.

Dewey CF, Bussolari SR, Gimbrone MA Jr, Davies PF. The dynamic response of vascular endothelial cells to fluid shear stress. J Biomech Eng. 1981;103:177–85.

Dineley J, Meagher S, Poepping TL, McDicken WN, Hoskins PR. Design and characterisation of a wall motion phantom. Ultrasound Med Biol. 2006;32:1349–57.

Doyle BJ, Morris LG, Callanan A, Kelly P, Vorp DA, McGloughlin TM. 3D reconstruction and manufacture of real abdominal aortic aneurysms: from CT scan to silicone model. J Biomech Eng. 2008;130:034501.

Friedman MH. Arteriosclerosis research using vascular flow models—from 2-d branches to compliant replicas. J Biomech Eng. 1993;115:595–601.

Friedman MH, Bargeron CB, Deters OJ, Hutchins GM, Mark FF. Correlation between wall shear and intimal thickness at a coronary artery branch. Atherosclerosis. 1987;68:27–33.

Gambillara V, Chambaz C, Montorzi G, Roy S, Stergiopulos N, Silacci P. Plaque-prone hemodynamics impair endothelial function in pig carotid arteries. Am J Physiol Heart Circ Physiol. 2006;290:H2320–8.

Gan L, Sjögren LS, Doroudi R, Jern S. A new computerized biomechanical perfusion model for ex vivo study of fluid mechanical forces in intact conduit vessels. J Vasc Res. 1999;36:68–78.

Geoghegan P, Buchmann N, Spence C, Moore S, Jermy M. Fabrication of rigid and flexible refractive-index-matched flow phantoms for flow visualisation and optical flow measurements. Exp Fluids. 2012;52:1331–47.

Han HC, Ku DN. Contractile responses in arteries subjected to hypertensive pressure in seven-day organ culture. Ann Biomed Eng. 2001;29:467–75.

Hattori K, Ikemoto Y, Takao W, Ohno S, Harimoto T, Kanazawa S, Oita M, Shibuya K, Kuroda M, Kato H. Development of MRI phantom equivalent to human tissues for 3.0-T MRI. Med Phys. 2013;40(3):032303. doi:10.1118/1.4790023.

Hellerbach A, Schuster V, Jansen A, Sommer J. MRI phantoms—are there alternatives to agar? PLoS ONE. 2013;8:e70343. doi:10.1371/journal.pone.0070343.

Hoskins PR. Simulation and validation of arterial ultrasound imaging and blood flow. Ultrasound Med Biol. 2008;34:693–717.

IEC 61685. Ultrasonics—flow measurement systems: flow test object. International Electrotechnical Commission, Geneva, Switzerland, 2001.

Kato H, Kuroda M, Yoshimura K, Yoshida A, Hanamoto K, Kawasaki S, Shibuya K, Kanazawa S. Composition of MRI phantom equivalent to human tissues. Med Phys. 2005;32:3199–208.

Kenwright DA, Laverick N, Anderson T, Moran CM, Hoskins PR. A wall-less flow phantom for high-frequency ultrasound applications. Ultrasound Med Biol. 2015;41:890–7.

King DM, Fagan AJ, Moran CM, Browne JE. Comparative imaging study in ultrasound, MRI, CT, and DSA using a multimodality renal artery phantom. Med Phys. 2011;38:565–73.

Kohler U, Marshall I, Robertson MB, Long Q, Xu Y, Hoskins PR. MRI measurement of wall shear stress in bifurcation models and comparison with CFD predictions. J Magn Reson Imaging. 2001;14:563–73.

Krueger JW, Young DF, Cholvin NR. An in vitro study of flow response by cells. J Biomech. 1971;4:31–6.

Ku DN, Giddens DP. Pulsatile flow in a model carotid bifurcation. Arteriosclerosis. 1983;3:313–9.

Lai SS, Yiu BY, Poon AK, Yu AC. Design of anthropomorphic flow phantoms based on rapid prototyping of compliant vessel geometries. Ultrasound Med Biol. 2013;39:1654–64.

Levesque MJ, Nerem RM. The elongation and orientation of cultured endothelial cells in response to shear stress. J Biomedl Eng. 1985;107:341.

Liepsch D, Pflugbeil G, Matsuo T, Lesniak B. Flow visualization and 1- and 3-D laser-Doppler-anemometer measurements in models of human carotid arteries. Clin Hemorheol Microcirc. 1998;18:1–30.

Mano I, Goshima H, Nambu M, Iio M. New polyvinyl-alcohol gel material for MRI phantoms. Magn Reson Med. 1986;3:921–6.

Marshall I. Computational simulations and experimental studies of 3D phase-contrast imaging of fluid flow in carotid bifurcation geometries. J Magn Reson Imaging. 2010;31:928–34.

Meagher S, Poepping TL, Ramnarine KV, Black RA, Hoskins PR. Anatomical flow phantoms of the nonplanar carotid bifurcation, part II. Experimental validation. Ultrasound Med Biol. 2007;33:303–10.

Miller P, Danielson K, Moody G, Slifka A, Drexler E, Hertzberg J. Matching index of refraction using a diethyl phthalate/ethanol solution for in vitro cardiovascular models. Exp Fluids. 2006;41:375–81.

Nguyen TT, Biadillah Y, Mongrain R, Brunette J, Tardif JC, Bertrand OF. A method for matching the refractive index and kinematic viscosity of a blood analog for flow visualization in hydraulic cardiovascular models. J Biomech Eng. 2004;126:529–35.

Ozaki H, Karaki H. Organ culture as a useful method for studying the biology of blood vessels and other smooth muscle tissues. Jpn J Pharmacol. 2002;89:93–100.

Prasad AK. Particle image velocimetry. Curr Sci. 2000;79:51–60.

Ramnarine KV, Nassiri DK, Hoskins PR, Lubbers J. Validation of a new blood mimicking fluid for use in Doppler flow test objects. Ultrasound Med Biol. 1998;24:451–9.
Ramnarine KV, Anderson T, Hoskins PR. Construction and geometric stability of physiological flow rate wall-less stenosis phantoms. Ultrasound Med Biol. 2001;32:245–50.
Robertson MB, Kohler U, Hoskins PR, Marshall I. Quantitative analysis of PC MRI velocity maps: pulsatile flow in cylindrical vessels. Mag Res Imag. 2001;19:685–95.
Rosen L, Hollis TM, Sharma MG. Document Alterations in bovine endothelial histidine decarboxylase activity following exposure to shearing stresses. Exp Molec Path. 1974;20: 329–43.
Smith RF, Rutt BK, Holdsworth DW. Anthropomorphic carotid bifurcation phantom for MRI applications. J Magn Reson Imaging. 1999;10:533–44.
Selwyn R. Phantoms for magnetic resonance imaging. In: DeWerd LA, Kissick M, editors. The phantoms of medical and health physics: devices for research and development. New York: Springer; 2014. p. 181–200.
Surry KJM, Austin HJB, Fenster A, Peters TM. Poly(vinyl alcohol) cryogel phantoms for use in ultrasound and MR imaging. Phys Med Biol. 2004;49:5529–46.
Steinman DA, Poepping TL, Tambasco M, Rankin RN, Holdsworth DW. Flow patterns at the stenosed carotid bifurcation: effect of concentric versus eccentric stenosis. Ann Biomed Eng. 2000;28:415–23.
Summers PE, Holdsworth DW, Nikolov HN, Rutt BK, Drangova M. Multisite trial of MR flow measurement: phantom and protocol design. J Magn Reson Imaging. 2005;21:620–31.
Teirlinck CJPM, Bezemer RA, Kollman C, Lubbers J, Hoskins PR, Fish P, Fredfeldt KE, Schaarschmidt UG. Development of an example flow test object and comparison of five of these test objects in various laboratories. Eur J Ultrasound. 1998;36:653–60.
Thacher TN, Silacci P, Stergiopulos N, da Silva RF. Autonomous effects of shear stress and cyclic circumferential stretch regarding endothelial dysfunction and oxidative stress: an ex vivo arterial model. J Vasc Res. 2010;47:336–45.
Tropea C. Laser Doppler anemometry: recent developments and future challenges. Meas Sci Technol. 1995;6:605–19.
Vennemann P, Lindken R, Westerweel J. In vivo whole-field blood velocity measurement techniques. Exp Fluids. 2007;42:495–511.
Virchow R. Der ateromatose Prozess der Arterien. Wien Med Wochenshr. 1856;6:825–41.
Watts DM, Sutcliffe CJ, Morgan RH, Ramnarine KV, Bastin M, Marshall I, Wardlaw J, Connell M, Hoskins PR, Black RA. Anatomical flow phantoms of the nonplanar carotid bifurcation I. Design. Ultrasound Med Biol. 2007;33:296–302.
Westerweel J. Fundamentals of digital particle image velocimetry. Meas Sci Technol. 1997;8:1379–92.
Young EW, Simmons CA. Macro- and microscale fluid flow systems for endothelial cell biology. Lab Chip. 2010;10:143–60.
Yousif MY, Holdsworth DW, Poepping TL. A blood-mimicking fluid for particle image velocimetry with silicone vascular models. Exp Fluids. 2011;50:769–74.
Zarins CK, Giddens DP, Bharadvaj BK, Sottiurai VS, Mabon RF, Glagov S. Carotid bifurcation atherosclerosis. Quantitative correlation of plaque localization with flow velocity profiles and wall shear stress. Circ Res. 1983;53:502–14.